J|A|C|S
ARTICLES
Published on Web 01/03/2004

Band-Selective Carbonyl to Aliphatic Side Chain $^{13}C-^{13}C$ Distance Measurements in U-^{13}C,^{15}N-Labeled Solid Peptides by Magic Angle Spinning NMR

Vladimir Ladizhansky and Robert G. Griffin*

Contribution from the Department of Chemistry and Center for Magnetic Resonance, Francis Bitter Magnet Laboratory, Massachusetts Institute of Technology, Cambridge, Massachusetts 02139-4307

Received July 8, 2003; E-mail: rgg@mit.edu

Abstract: We describe three-dimensional magic angle spinning NMR experiments that enable simultaneous band-selective measurement of the multiple distance constraints between carbonyl and side chain carbons in uniformly ^{13}C,^{15}N-labeled peptides. The approaches are designed to circumvent the dipolar truncation and to allow experimental separation of the multiple quantum (MQ) relaxation and dipolar effects. The pulse sequences employ the double quantum (DQ) rotational resonance in the tilted frame (R^2TR) to perform selective polarization transfers that reintroduce the $^{13}C'-^{13}C\gamma,\delta$ dipolar interactions. The scheme avoids recoupling of the strongly coupled $C'-C\alpha$ and $C'-C\beta$ spin pairs, therefore minimizing dipolar truncation effects. The experiment is performed in a constant time fashion as a function of the radio frequency irradiation intensity and measures the line shape of the DQ transition. The width and the intensity of this line shape are analyzed in terms of the DQ relaxation and dipolar coupling. The attenuation of the multispin effects in the presence of relaxation enables a two-spin approximation to be employed for the analysis of the experimental data. The systematic error introduced by this approximation is estimated by comparing the results with a three-spin simulation. The contributions of B_1-inhomogeneity, CSA orientation effects, and the effects of inhomogeneous line broadening are also estimated. The experiments are demonstrated in model U-^{13}C,^{15}N-labeled peptides, *N*-acetyl-L-Val-L-Leu and *N*-formyl-L-Met-L-Leu-L-Phe, where 10 and 6 distances, ranging between 3 and 6 Å, were measured, respectively.

Introduction

Solid-state NMR (ssNMR) is a rapidly developing tool for structure determinations in biological solids.[1−5] To achieve the spectral resolution required to perform measurements in a site-specific manner, the application of magic angle spinning (MAS) techniques is usually required.[6,7] MAS removes dominant chemical shift anisotropy interactions, but concurrently attenuates the dipolar couplings that contain information about internuclear distances. This information can, however, be reintroduced in a controlled manner by dipolar recoupling techniques, and the dipolar interactions and therefore distances can be quantified.[8,9] In the past, the main focus of ssNMR structural studies has been exclusively on samples with specific isotopically labeled sites.[10−15] More recently, several research groups initiated studies exploring the possibility of acquiring multiple structural constraints in uniformly labeled solids with the goal of complete structure determination in peptides and proteins.[5,16−27] In such samples, a large number of geometrical

(1) Griffin, R. G. *Nat. Struct. Biol.* **1998**, *5*, 508−512.
(2) Tycko, R. *Annu. Rev. Phys. Chem.* **2001**, *52*, 575−606.
(3) Opella, S. J. *Nat. Struct. Biol.* **1997**, *4*, 845−848.
(4) Watts, A. *Curr. Opin. Biotechnol.* **1999**, *10*, 48−53.
(5) Castellani, F.; van Rossum, B.-J.; Diehl, A.; Schubert, M.; Rehbein, K.; Oschkinat, H. *Nature* **2002**, *420*, 98−102.
(6) Lowe, I. J. *Phys. Rev. Lett.* **1959**, *2*, 285.
(7) Andrew, E. R.; Bradbury, A.; Eades, R. G. *Nature* **1958**, *182*, 1659.
(8) Bennett, A. E.; Griffin, R. G.; Vega, S. Recoupling of homo- and heteronuclear dipolar interactions in rotating solids. In *Solid State NMR IV: Methods and Applications of Solid-State NMR*; Blumich, B., Ed.; Springer-Verlag: Berlin, 1994; pp 1−77.
(9) Dusold, S.; Sebald, A. *Annu. Rep. NMR Spectrosc.* **2000**, *41*, 185−264.
(10) McDermott, A.; Creuzet, F.; Gebhard, R.; van der Hoef, K.; Levitt, M. H.; Herzfeld, J.; Lugtenburg, J.; Griffin, R. G. *Biochemistry* **1994**, *33*, 6129−6136.
(11) McDermott, A.; Creuzet, F.; Griffin, R. G.; Zawadzke, L. E.; Ye, Q. Z.; Walsh, C. T. *Biochemistry* **1990**, *29*, 5567−5574.
(12) McDowell, L. M.; Klug, C. A.; Beusen, D. D.; Schaefer, J. *Biochemistry* **1996**, *35*, 5395−5403.
(13) Creuzet, F.; McDermott, A.; Gebhard, R.; van der Hoef, K.; Spijker-Assink, M. B.; Herzfeld, J.; Lugtenburg, J.; Levitt, M. H.; Griffin, R. G. *Science* **1991**, *251*, 783−786.
(14) Feng, X.; Verdegem, P. J. E.; Eden, M.; Sandstrom, D.; Lee, Y. K.; BoveeGeurts, P. H. M.; Grip, W. J. d.; Lugtenburg, J.; Groot, H. J. M. d.; Levitt, M. H. *J. Biomol. NMR* **2000**, *16*, 1−8.
(15) Lansing, J. C.; Hohwy, M.; Jaroniec, C. P.; Creemers, A. F. L.; Lugtenburg, J.; Herzfeld, J.; Griffin, R. G. *Biochemistry* **2002**, *41*, 431−438.
(16) Hong, M. *J. Biomol. NMR* **1999**, *15*, 1−14.
(17) Nomura, K.; Takegoshi, K.; Terao, T.; Uchida, K.; Kainosho, M. *J. Am. Chem. Soc.* **1999**, *121*, 4064−4065.
(18) McDermott, A.; T. Polenova, T.; Bockmann, A.; Zilm, K. W.; Paulsen, E. K.; Martin, R. W.; Montelione, G. T. *J. Biomol. NMR* **2000**, *16*, 209−219.
(19) Nomura, K.; Takegoshi, K.; Terao, T.; Uchida, K.; Kainosho, M. *J. Biomol. NMR* **2000**, *17*, 111−123.
(20) Detken, A.; Hardy, E. H.; Ernst, M.; Kainosho, M.; Kawakami, T.; Aimoto, S.; Meier, B. H. *J. Biomol. NMR* **2001**, *20*, 203−221.
(21) Pauli, J.; Baldus, M.; van Rossum, B.-J.; de Groot, H. J. M.; Oschkinat, H. *Chembiochem.* **2001**, *2*, 272−281.
(22) van Rossum, B.-J.; Castellani, F.; Rehbein, K.; Pauli, J.; Oschkinat, H. *Chembiochem.* **2001**, *2*, 906−914.
(23) Rienstra, C. M.; Hohwy, M.; Mueller, L. J.; Jaroniec, C. P.; Reif, B.; Griffin, R. G. *J. Am. Chem. Soc.* **2002**, *124*, 11908−11922.
(24) Rienstra, C. M.; Tucker-Kellogg, L.; Jaroniec, C. P.; Hohwy, M.; Reif, B.; McMahon, M. T.; Tidor, B.; Lozano-Perez, T.; Griffin, R. G. *Proc. Natl. Acad. Sci. U.S.A.* **2002**, *99*, 10260−10265.

10.1021/ja037138c CCC: $27.50

constraints can, in principle, be collected, and the main focus of research has been the development of the efficient approaches to accomplish this end. The methods currently available include (i) a large suite of dipolar correlation experiments for the measurements of the backbone and side chain torsion angles ϕ, ψ, and χ,[23,25,28−32] and (ii) methods for simultaneous determination of multiple $^{13}C-^{15}N$ distances.[33] In this publication, we will focus our attention on the problem of homonuclear $^{13}C-^{13}C$ recoupling in uniformly labeled spin systems with the ultimate goal of the simultaneous measurement of multiple $^{13}C-^{13}C$ distances.

A number of recoupling experiments have been developed to reintroduce $^{13}C-^{13}C$ dipolar interactions during MAS.[8,9,34−39] These methods are conveniently classified into two categories: broadband methods designed to recouple all spins independent of their chemical shifts,[34−36] and selective methods,[37−39] where the recoupling efficiency is a strong function of the relative positions of the spectral lines. Broadband recoupling sequences are specifically designed to eliminate the influence of the chemical shift terms and reintroduce all dipolar couplings in the system. This is highly desirable for sequential spectral assignment experiments, which exploit the polarization transfer over strong one-bond couplings. In the case of broadband recoupling, however, the system behaves as a continuous network of dipolar-coupled spins, where strong one- and two-bond dipolar interactions dominate the weak, structurally important couplings. This, in turn, leads to dipolar truncation effects[35,40−43] and makes long-range distance measurements a complicated task. In contrast, selective recoupling methods reintroduce dipolar interactions between nuclei with defined spectroscopic parameters—isotropic chemical shifts. For example, in rotational resonance (R^2) experiments,[37] efficient recoupling is achieved if the chemical shift difference between recoupled spins, δ, matches a small integer multiple of the spinning frequency, $\delta = n\nu_r$. If this condition is fulfilled, a resonant exchange of energy is established between the mechanical sample rotation and the nuclear spins, and the homonuclear dipolar interaction has a significant effect on the spin dynamics. Other spins whose isotropic chemical shifts do not satisfy the R^2 matching condition are affected to a much smaller extent.[44]

Similar effects are also observed in the selective recoupling experiments exploiting rotational resonance in the tilted frame (R^2TR) under the influence of the weak radio frequency (rf) irradiation.[38,39,45] In these experiments, the resonance condition is established in the tilted frame defined by the isotropic chemical shifts and rf terms in the Hamiltonian. Similar to R^2, the R^2TR[38,39] matching conditions depend strongly on the chemical shifts of recoupled nuclear spins, and by appropriately choosing the carrier position, spinning frequency, and the rf intensity, one can establish selective magnetization exchange between specific carbon spins. Concurrently, the spinning frequency can be chosen to avoid R^2 conditions and the line broadening usually associated with it. Conceptually, at least, due to their selectivity, the R^2 and R^2TR techniques can be used to reintroduce dipolar interactions in a pairwise fashion, even in uniformly labeled sample. This allows one to avoid recoupling of strong one- and two-bond interactions and attenuates dipolar truncation.

Another problem arises from the fact that the recoupling effects are also a strong function of multiple-quantum (MQ) relaxation rates.[46] ZQ relaxation effects have been studied in detail in the framework of R^2 recoupling.[46−49] In cases when the relaxation rate is slower than the effective dipolar interaction, the dipolar and relaxation effects can be easily distinguished.[44,46] However, in the opposite "overdamped" regime,[46] the interpretation of the experiments may result in ambiguities in the measured distances. Although experiments have been devised to measure zero quantum (ZQ) relaxation contributions to the magnetization decay,[47] the relaxation effects are not easy to separate experimentally in recoupling experiments involving rf fields, and their measurement is likely to be even more complicated in multispin systems. On the other hand, it has been shown[48] that simple models widely used to estimate MQ relaxation may result in incorrect predictions and, as a result, in optimistic estimates of the accuracy of the distance measurements.

There have been a number of attempts to design recoupling methods that are less sensitive to MQ relaxation[45,50] or allow independent extraction of the relaxation rate along with dipolar coupling.[51−53] In particular, the related narrow-band spin−echo dipolar recoupling (nb-SEDRA), narrow-band radio frequency driven dipolar recoupling (nb-RFDR),[51,52] and the rotational

(25) Ladizhansky, V.; Jaroniec, C. P.; Diehl, A.; Oschkinat, H.; Griffin, R. G. *J. Am. Chem. Soc.* **2003**, *125*, 6827−6833.
(26) Egorova-Zachernyuk, T. A.; Hollander, J.; Fraser, N.; Gast, P.; Hoff, A. J.; Cogdell, J.; de Groot, H. J. M.; Baldus, M. *J. Biomol. NMR* **2001**, *19*, 243−253.
(27) Jaroniec, C. P.; Tounge, B. A.; Herzfeld, J.; Griffin, R. G. *J. Am. Chem. Soc.* **2001**, *123*, 3507−3519.
(28) Feng, X.; Lee, Y. K.; Sandström, D.; Eden, M.; Maisel, H.; Sebald, A.; Levitt, M. H. *Chem. Phys. Lett.* **1996**, *257*, 314−320.
(29) Feng, X.; Eden, M.; Brinkmann, A.; Luthman, H.; Eriksson, L.; Gräslund, A.; Antzutkin, O. N.; Levitt, M. H. *J. Am. Chem. Soc.* **1997**, *119*, 12006−12007.
(30) Costa, P. R.; Gross, J. D.; Hong, M.; Griffin, R. G. *Chem. Phys. Lett.* **1997**, *280*, 95−103.
(31) Hong, M.; Gross, J. D.; Griffin, R. G. *J. Phys. Chem. B* **1997**, *101*, 5869−5874.
(32) Ladizhansky, V.; Veshtort, M.; Griffin, R. G. *J. Magn. Reson.* **2002**, *154*, 317−324.
(33) Jaroniec, C. P.; Filip, C.; Griffin, R. G. *J. Am. Chem. Soc.* **2002**, *124*, 10728−10742.
(34) Rienstra, C. M.; Hatcher, M. E.; Mueller, L. J.; Sun, B. Q.; Fesik, S. W.; Griffin, R. G. *J. Am. Chem. Soc.* **1998**, *120*, 10602−10612.
(35) (a) Hohwy, M.; Jakobsen, H. J.; Eden, M.; Levitt, M. H.; Nielsen, N. C. *J. Chem. Phys.* **1998**, *108*, 2686−2694. (b) Hohwy, M.; Rienstra, C. M.; Jaroniec, C. P.; Griffin, R. G. *J. Chem. Phys.* **1999**, *110*, 7983−7992.
(36) Brinkmann, A.; Edén, M.; Levitt, M. H. *J. Chem. Phys.* **2000**, *112*, 8539−8554.
(37) Raleigh, D. P.; Levitt, M. H.; Griffin, R. G. *Chem. Phys. Lett.* **1988**, *146*, 71−76.
(38) Takegoshi, K.; Nomura, K.; Terao, T. *Chem. Phys. Lett.* **1995**, *232*, 424−428.
(39) Takegoshi, K.; Nomura, K.; Terao, T. *J. Magn. Reson.* **1997**, *127*, 206−216.
(40) Hodgkinson, P.; Emsley, L. *J. Magn. Reson.* **1999**, *139*, 46−59.
(41) Hohwy, M.; Rienstra, C. M.; Griffin, R. G. *J. Chem. Phys.* **2002**, *117*, 4973−4987.
(42) Ladizhansky, V.; Vega, S. *J. Chem. Phys.* **2000**, *112*, 7158−7166.
(43) Ladizhansky, V.; Vinogradov, E.; van Rossum, B.-J.; de Groot, H. J. M.; Vega, S. *J. Chem. Phys.* **2003**, *118*, 5547−5557.
(44) Williamson, P. T. F.; Verhoeven, A.; Ernst, M.; Meier, B. H. *J. Am. Chem. Soc.* **2003**, *125*, 2718−2722.
(45) Costa, P. R.; Sun, B.; Griffin, R. G. *J. Am. Chem. Soc.* **1997**, *119*, 10821−10836.
(46) Levitt, M. H.; Raleigh, D. P.; Creuzet, F.; Griffin, R. G. *J. Chem. Phys.* **1990**, *92*, 6347−6364.
(47) Karlsson, T.; Levitt, M. H. *J. Chem. Phys.* **1998**, *109*, 5493−5507.
(48) Karlsson, T.; Brinkmann, A.; Verdegem, P. J. E.; Lugtenburg, J.; Levitt, M. H. *Solid State Nucl. Magn. Reson.* **1999**, *14*, 43−58.
(49) Helmle, M.; Lee, Y. K.; Verdegem, P. J. E.; Feng, X.; Karlsson, T.; Lugtenburg, J.; de Groot, H. J. M.; Levitt, M. H. *J. Magn. Reson.* **1999**, *140*, 379−403.
(50) Bennett, A. E.; Weliky, D. P.; Tycko, R. *J. Am. Chem. Soc.* **1998**, *120*, 4897−4898.
(51) Goobes, G.; Boender, G. J.; Vega, S. *J. Magn. Reson.* **2000**, *146*, 204−219.
(52) Goobes, G.; Vega, S. *J. Magn. Reson.* **2002**, *146*, 236−251.
(53) Costa, P. R.; Sun, B.; Griffin, R. G. *J. Magn. Reson.* **2003**, *164*, 92−103.

resonance width (R^2W)[53] experiments are conducted as a function of spinning frequency, and the width and the depth of the ZQ transition are measured as a function of the deviation from the exact rotational resonance condition. The dipolar coupling and relaxation rate can be extracted from the resulting resonance shape independently. These "resonance width" approaches only assume the exponential character of the relaxation of multiple quantum coherences and do not require a knowledge of the multiple quantum relaxation parameter. Therefore, they lead to an unambiguous estimation of the dipolar couplings.

In this paper, we describe a constant time band-selective 3D R^2TR width (R^2TRW) method for $^{13}C-^{13}C$ distance measurements that is designed to address problems associated with the dipolar truncation effects and multiple quantum relaxation. In contrast to nb-SEDRA, nb-RFDR, and R^2W methods, the experiments presented here are based on the R^2TR^{38} technique and can be performed at spinning frequencies mismatched from the R^2 condition. Therefore, R^2 effects do not affect the resolution of the ^{13}C spectra. The method can be combined with either $^{13}C-^{13}C$ or $^{13}C-^{15}N$ correlation spectroscopy for site-specific resolution and allows site-specific extraction of distances between carbonyl and side chain carbons. We demonstrate the technique in U-^{13}C,^{15}N-labeled peptides *N*-acetyl-[U-^{13}C,^{15}N]-L-Val-L-Leu and *N*-formyl-[U-^{13}C,^{15}N]L-Met-L-Leu-L-Phe where 10 and 6 intra- and interresidue carbonyl−side chain $^{13}C-^{13}C$ distances in a range of 2.9−6 Å were measured, respectively. We used a simple two-spin approximation to analyze data and estimated the systematic errors associated with the use of this simplified model. Other sources of systematic error are discussed as well.

Experimental Section

Uniformly Labeled Peptides. The peptides used in the experiments were *N*-acetyl-[U-^{13}C,^{15}N]L-Val-L-Leu (N-Ac-VL) and *N*-formyl-[U-^{13}C,^{15}N]L-Met-L-Leu-L-Phe (N-*f*-MLF-OH). The synthetic procedures were described elsewhere.[27,54,55] To minimize the effects of intermolecular couplings, N-Ac-VL and N-*f*-MLF-OH peptides were recrystallized from the solutions diluted to 9% and 10%, respectively, in the respective natural abundance peptides.

NMR Experiments. NMR experiments were performed on custom-designed spectrometers designed by Dr. David J. Ruben, at 11.7 T (500.125 MHz for ^1H, 125.7 MHz for ^{13}C, and 50.6 MHz for ^{15}N, respectively) and at 8.42 T (360.306 MHz for ^1H, 90.603 MHz for ^{13}C, and 36.43 MHz for ^{15}N, respectively), both equipped with 4-mm triple resonance Chemagnetics (Fort Collins, CO) probes. The experiments on N-Ac-VL were performed on the 360 MHz instrument at a spinning frequency of 7.4 kHz. The experiments on N-*f*-MLF-OH were performed on the 500 MHz spectrometer at a spinning frequency of 10.5 kHz. The spinning rates were controlled with Bruker spinning frequency controllers to a stability of ±2 Hz.

Two pulse sequences have been used in the experiments. The pulse sequence for the 3D R^2TRW experiment shown in Figure 1a combines dipolar recoupling with $^{13}C-^{13}C$ correlation spectroscopy.

Here, the initial excitation by cross polarization (CP)[57] is implemented on the ^{13}C channel and followed by frequency labeling during t_1. The t_1 evolution period concludes with a strong $\pi/2$ pulse that restores the magnetization to a longitudinal direction. This is followed by a "ramp up" period, during which the polarizations of different ^{13}C's are aligned in their respective tilted frames for polarization transfer, which takes place during the constant mixing time period. During this period, the weak rf field of a variable intensity is applied, defining the third dimension of the experiment. This leads to a buildup of $^{13}C'-^{13}C\gamma,\delta$ cross-peaks, whose intensities depend strongly on the rf strength, dipolar interactions between the corresponding spins, and relaxation parameters. The mixing period is followed by a "ramp down" period, during which the rf power is gradually decreased, thus causing the directions of the effective fields to align in the longitudinal direction in the laboratory frame. At the end of the "ramp down" period, all carbonyl and side chain magnetizations are aligned along the *z*-axis and can be detected after a nonselective $\pi/2$ pulse.

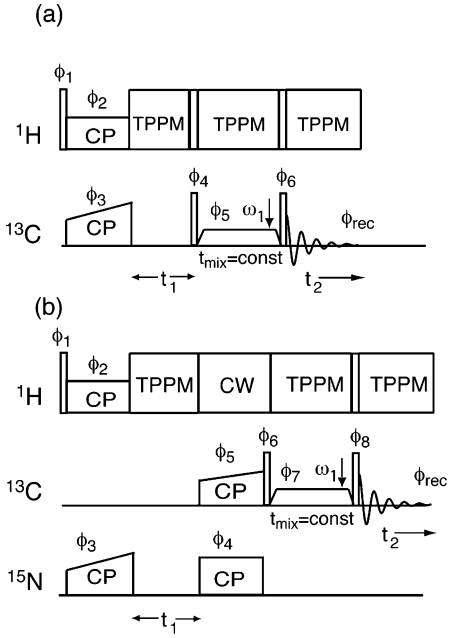

Figure 1. Three-dimensional $^{13}C-^{13}C$ R^2TRW (a) and $^{13}C-^{15}N$ R^2TRW (b) chemical shift dipolar correlation pulse sequences. Open rectangles represent $\pi/2$ pulses. In (a), following ^1H to ^{13}C CP, the magnetization evolves under the chemical shifts, and then is prepared along the tilted axes by a $\pi/2$ pulse and ramp up period. The carbonyl to side chain polarization transfer takes place during the constant mixing period t_{mix}. The phase cycles in (a) were $\phi_1 = 8 \times 1\ 8 \times 3$, $\phi_2 = 4$, $\phi_3 = 13243142$, $\phi_4 = 22334411\ 44112233$, $\phi_5 = 11223344\ 33441122$, $\phi_6 = 22334411\ 44112233$, $\phi_{rec} = 13243142\ 31421324$, where $1 = x$, $2 = y$, $3 = -x$, $4 = -y$. Hypercomplex data were acquired by shifting ϕ_4 according to Ruben and co-workers.[56] In (b), the ^1H to ^{15}N CP creates $^{15}N_{i+1}$ magnetization that evolves under the chemical shifts. The magnetization is transferred selectively to $^{13}C'$ carbons and prepared along their tilted axes by a hard $\pi/2$ and ramp up period. The dipolar contact is established during the constant mixing time t_{mix}. The phase cycles in (b) were: $\phi_1 = 8 \times 1\ 8 \times 3$, $\phi_2 = 4$, $\phi_3 = 4 \times (13)$, $\phi_4 = 1$, $\phi_5 = 11223344$, $\phi_6 = 22334411\ 44112233$, $\phi_7 = 22334411\ 44112233$, $\phi_8 = 22334411\ 44112233$, $\phi_{rec} = 13243142\ 31421324$. Hypercomplex data were acquired by shifting ϕ_4.

The pulse sequence in Figure 1b is based on similar principles, with the exception that the initial excitation and t_1 evolution periods are implemented on the ^{15}N channel to enhance spectral resolution. It results in a series of 2D $^{15}N-^{13}C$ correlation spectra, with cross-peak intensities that are a function of the rf strength, dipolar coupling, and multiple quantum relaxation. Following the $^1H-^{15}N$ CP period, the ^{15}N magnetization is frequency labeled in the t_1 dimension. The magnetization is then transferred to carbonyl carbons by selective $^{15}N-^{13}C$ cross polarization where the ^{13}C and ^{15}N channel rf intensities and resonance offsets were adjusted to ensure the band-selective $^{15}N_{i+1}-C'_i$ transfer.[58] The nonselective $\pi/2$ pulse aligns the magnetization along the *z*-axis, and the remainder of the experiment is identical to that in Figure 1a.

(54) Stewart, P. L.; Tycko, R.; Opella, S. J. *J. Chem. Soc., Faraday Trans. 1* **1988**, *84*, 3803−3819.
(55) Rienstra, C. M.; Hohwy, M.; Hong, M.; Griffin, R. G. *J. Am. Chem. Soc.* **2000**, *122*, 10979−10990.
(56) States, D. J.; Haberkorn, R. A.; Ruben, D. J. *J. Magn. Reson.* **1982**, *48*, 286−292.
(57) Pines, A.; Gibby, M. G.; Waugh, J. S. *J. Chem. Phys.* **1973**, *59*, 569−590.

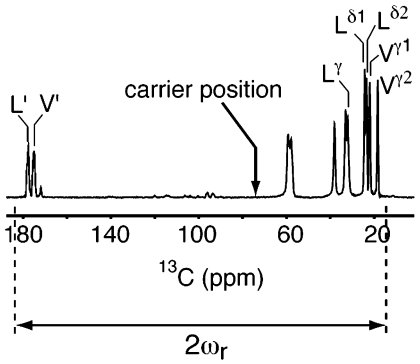

Figure 2. One-dimensional ^{13}C spectrum of *N*-Ac-[^{13}C,^{15}N]VL with a typical choice of the carrier position and the spinning frequency in the R^2-TRW experiment. Application of the weak rf field results in matching the $n = 2$ DQ R^2TR conditions for CO−Cγ,δ carbons and establishes polarization transfer between them.

The choice of the spinning frequency and carrier position is illustrated for typical experimental circumstances in Figure 2.

The ^{13}C $\pi/2$ pulses were 5 μs, the ramp up and ramp down periods were 0.5 ms, and the TPPM[59] decoupling during t_1, ramp up, ramp down, dipolar mixing t_{mix}, and acquisition t_2 periods was adjusted to ~83 kHz (total phase difference 12°; TPPM pulse length, 6 μs). The CW decoupling field during the ^{13}C $\pi/2$ pulses and $^{15}N-^{13}C$ CP was 100 kHz.

Theory and Simulations

In this section, we discuss the spin dynamics during the mixing time. We first derive the time-independent effective dipolar Hamiltonian in a form best suited for our experimental conditions and then analyze various sources of systematic errors associated with the approximate theoretical model. We consider a system of *n* homonuclear spins coupled by dipolar interactions. The Hamiltonian of this system can be written as

$$H = -\omega_1 S_x - \sum_i \Delta\omega_i S_{iz} - \sum_i \omega_i^{(csa)}(t) S_{iz} + \sum_{i<j} \omega_{ij}^D(t)(3S_{iz}S_{jz} - \boldsymbol{S_i}\cdot\boldsymbol{S_j})$$

$$\omega_{ij}^D(t) = \sum_{n=-2}^{n=2} d_{ij}^{(n)} e^{in\omega_R t},$$

$$\omega_i^{(csa)}(t) = \sum_{n=-2}^{n=2} \omega_{in}^{(csa)} e^{in\omega_R t} \quad (1)$$

where the first term describes the weak C.W. radio frequency field, the second and the third terms describe the isotropic and anisotropic chemical shift interactions, respectively, and the last term corresponds to the homonuclear dipolar interactions between the spins. The expressions for the CSA and dipolar coefficients $d_{ij}^{(n)}$, $\omega_{in}^{(csa)}$ are given elsewhere.[8] To derive the time-independent effective Hamiltonian, two transformations are required.[38,39] The first transformation to the tilted frame is achieved by applying the rotation

$$U_1 = \exp(i\sum_j \beta_j S_{jy}) \quad (2)$$

where tilted angles are defined as $\beta_j = \arctan(\omega_1/\Delta\omega_j)$. The transformed tilted frame Hamiltonian becomes:

$$\tilde{H} = \tilde{H}_Z + \tilde{H}_{CSA} + \tilde{H}_{dip}$$

$$\tilde{H}_Z = -\sum_i \omega_i^{eff} S_{iz}$$

$$\tilde{H}_{CSA} = \sum_i \omega_i^{(csa)}(t)\{-S_{iz}\cos\beta_i + S_{ix}\sin\beta_i\}$$

$$\tilde{H}_{dip} = \sum_{i<j} \omega_{ij}^D(t)\begin{Bmatrix} A_{ij}S_{iz}S_{jz} + B_{ij}(S_i^+S_j^- + S_i^-S_j^+) + R_{ij}S_{iz}S_j^\pm + \\ Q_{ij}(S_i^+S_j^+ + S_i^-S_j^-) + K_{ij}S_{iz}^\pm S_{jz} \end{Bmatrix} \quad (3)$$

The effective field for each spin is a geometrical sum of the rf and the corresponding isotropic chemical shift terms

$$\omega_i^{eff} = \sqrt{\Delta\omega_i^2 + \omega_1^2} \quad (4)$$

and points in the direction of the respective tilted *z*-axis. The geometrical scaling factors for each spin pair are given as[38]

$$A_{ij} = -(2\cos\beta_i\cos\beta_j - \sin\beta_i\sin\beta_j)$$

$$B_{ij} = -\frac{1}{4}(1 + \cos\beta_i\cos\beta_j - 2\sin\beta_i\sin\beta_j)$$

$$R_{ij} = -\frac{1}{2}(2\cos\beta_i\sin\beta_j + \sin\beta_i\cos\beta_j)$$

$$K_{ij} = -\frac{1}{2}(2\sin\beta_i\cos\beta_j + \cos\beta_i\sin\beta_j)$$

$$Q_{ij} = \frac{1}{4}(1 + 2\sin\beta_i\sin\beta_j - \cos\beta_i\cos\beta_j) \quad (5)$$

Depending on the rf intensity, various matching conditions are possible. Two types of conditions can, in principle, occur:[38,39] the ZQ conditions for a (*i*,*j*)-spin pair occur at radio frequency intensities satisfying the equality

$$|\omega_i^{eff} - \omega_j^{eff}| = n\omega_R, \quad n = 1,2 \text{ (ZQ)} \quad (6a)$$

whereas the double quantum (DQ) conditions satisfy the equality

$$\omega_i^{eff} + \omega_j^{eff} = n\omega_R, \quad n = 1,2 \text{ (DQ)} \quad (6b)$$

The choice of the experimental parameters for the $n = 2$ DQ efficient recoupling of the carbonyl−side chain dipolar interactions is shown in Figure 2: (i) the spinning frequency is adjusted such that $n\omega_R$ ($n = 1,2$) just exceeds the largest chemical shift difference between the carbonyl resonances and the side chain resonances, $n\omega_R \geq \Delta\omega_{CO} - \Delta\omega_{side\ chain}$, (ii) the carrier frequency is set between these two groups of resonances to ensure favorable geometrical scaling factors Q_{ij} in eq 5, and (iii) the weak rf field is applied to satisfy the DQ condition (eq 6b). The recoupling of the $n = 2$ condition requires only moderate spinning frequencies (e.g., 10.5−11 kHz at a magnetic field of 500 MHz).

(58) Baldus, M.; Petkova, A. T.; Herzfeld, J.; Griffin, R. G. *Mol. Phys.* **1998**, *95*, 1197−1207.
(59) Bennett, A. E.; Rienstra, C. M.; M., A.; Lakshmi, K. V.; Griffin, R. G. *J. Chem. Phys.* **1995**, *103*, 6951−6957.

Under the experimental conditions of weak rf irradiation, the main contribution to the effective fields in eq 4 will be from the resonance offsets, and the directions of the effective field for carbonyl and side chain carbons will be close to the direction of the laboratory *z*-axis. This strong dependence on the chemical shift permits selective recoupling of the CO−Cγ,δ interactions, while Cα and Cβ spins, whose chemical shifts are very different from the chemical shifts of the outer aliphatic carbons, will not participate in the spin dynamics. Therefore, we can expect that the dipolar truncation effects will be minimized in this case.

In addition to CO−Cγ,δ recoupling conditions, other recoupling effects may occur. For example, under the experimental conditions of Figure 2, $n = 1$ DQ recoupling for side chain−side chain dipolar interactions may take place. These effects can potentially complicate the data interpretation, but can be avoided by choosing the carrier position to satisfy the condition $|\Delta\omega_{\text{side chain}}| + |\Delta\omega_{\text{side chain}}| > \omega_R$, which makes it impossible to fulfill the $n = 1$ DQ recoupling conditions between side chain resonances. On the other hand, the carrier position has to be far enough from the carbonyl lines to keep the tilted axis direction close to the laboratory frame *z*-axis. This minimizes the CSA component that is orthogonal to the direction of the tilted *z*-axis (this component is proportional to S_{ix} in eq 3) and minimizes decay of the carbonyl magnetization that would be associated with these terms. In the following, we assume that we can achieve perfectly selective carbonyl−side chain recoupling and other spin pairs will not participate in the spin dynamics. The additional magnetization decay that stems from the unwanted recoupling effects (for example, Cα−Cγ,δ) will be accounted for through the introduction of the effective longitudinal relaxation parameters in the tilted frame.

To derive the effective Hamiltonian adequately describing the carbonyl−side chain spin dynamics in the vicinity of the $n = 2$ DQ resonance condition, we will further transform the tilted frame Hamiltonian in eq 3 according to the transformation:

$$U_{\text{INT}} = \exp\{-i\sum_j (\omega_R t + \int_0^t \tilde{\omega}_j^{(\text{csa})}(t')\,dt')S_{jz}\} \qquad (7)$$

where the second term in the exponent describes the transformation into the interaction frame of the CSA. After the transformation, the dominant nonvanishing time-independent DQ term in the expression for the average Hamiltonian is:

$$H_{\text{eff}} = -\sum_i \Delta_i I_{iz} - \sum_j \Delta_j S_{jz} + \sum_{i,j} Q_{ij} D_{ij} (I_i^+ S_j^+ + I_i^- S_j^-) \quad (8)$$

where we now use I_p, S_p operators to distinguish carbonyl and side chain spins, respectively, and the indices *i* and *j* run over the carbonyl and side chain carbons. The coefficients Δ characterize the deviation from exact resonance and are

$$\Delta_i = \omega_i^{\text{eff}} - \omega_R \qquad (9)$$

and the influence of the transverse CSA component in eq 3 was neglected. The magnitude of this component is proportional to sin β ($\beta \approx 0°$) and, therefore, close to zero. The effective dipolar couplings are scaled due to the longitudinal terms of the CSA Hamiltonian $\tilde{\omega}_i^{(\text{csa})}(t) = \omega_i^{(\text{cas})}(t) \cos \beta_i$:

$$D_{ij} = \sum_{N=-2}^{N=2} I_{ij}^{(N)} d_{ij}^{(-N)}$$

$$I_{ij}^{(N)} = \sum\sum\sum\sum_{\substack{k,n,p,m,\\ k+2n+p+2m+2=N}} \times J_k(2|\omega_{i1}^{(\text{csa})}|\cos\beta_i/\omega_R) J_n(|\omega_{i2}^{(\text{csa})}|\cos\beta_i/\omega_R) \times J_p(2|\omega_{j1}^{(\text{csa})}|\cos\beta_j/\omega_R) J_m(|\omega_{j2}^{(\text{csa})}|\cos\beta_j/\omega_R) \quad (10)$$

where $J_k(x)$ are Bessel functions of the first kind, and the relation

$$\exp\{iz\sin\phi\} = \sum_{k=-\infty}^{k=\infty} \exp\{ik\phi\} J_k(z) \qquad (11)$$

was used for the calculation of eqs 8 and 10. To accommodate relaxation effects, it is convenient to use the Liouville−von Neumann equation of motion for the density matrix ρ of a given molecular orientation:[60]

$$\frac{d}{dt}\rho(t) = \hat{L}\rho(t) \qquad (12)$$

where the Liouville superoperator is defined as $\hat{L} = -i\hat{H}_{\text{eff}} - \hat{\Gamma}$. The matrix elements of the Hamiltonian commutation superoperator $\hat{H}_{\text{eff}}$ and of the diagonal relaxation superoperator $\hat{\Gamma}$ in the orthonormal basis set of operators $|Q_i\rangle$ are:[60]

$$(Q_i|\hat{H}_{\text{eff}}|Q_j) = Tr\{Q_i[H_{\text{eff}},Q_j]\}$$

$$(Q_i|\hat{\Gamma}|Q_j) = \frac{\delta_{ij}}{T_i} \qquad (13)$$

The parameters T_i denote relaxation times associated with the decay of coherences, Q_i. The use of the diagonal representation of the relaxation superoperator represents a model assumption and implies that the decay of the multiple-quantum coherences and of the longitudinal magnetization in the tilted frame is exponential.

The spin dynamics generated by the Hamiltonian in eq 8 can be approached in different ways. In one extreme, we can try to analyze the problem in its entirety, systematically varying the parameters that characterize the spin system − dipolar couplings and relaxation rates − and evaluate the RMS deviation from the experimental data. In some circumstances, this may not be a practical approach, because the number of parameters involved and the size of the problem become prohibitively large even for a small number of spins. Thus, further simplifications and approximations will be required. Another extreme may be the maximum simplification of the model used to analyze the data and accounting for the systematic error introduced by this simplification. In this work, we will pursue the second approach and use a two-spin approximation to analyze the spin dynamics. A more comprehensive treatment will be given in a future publication.

Two-Spin Approximation. In a two-spin approximation, all multiple dipolar interactions are neglected, and the effective Hamiltonian of eq 8 simplifies to

(60) Ernst, R. R.; Bodenhausen, G.; Wokaun, A. *Principles of Nuclear Magnetic Resonance in One and Two Dimensions*; Oxford: Clarendon Press, 1991.

$$H_{\text{eff}} = -\Delta_1 S_z - \Delta_2 I_z + \omega_D^{\text{eff}}(S^+ I^+ + S^- I^-) \qquad (14)$$

Equation 12 can be rewritten as a system of four homogeneous differential equations. We define this system in the subspace spanned by four orthonormal states $|Q_i\rangle$, where Q_i denotes spin operators

$$Q_1 = I_z, \quad Q_2 = S_z$$

$$Q_3 = \sqrt{2}(I^+ S^+ + I^- S^-)$$

$$Q_4 = -i\sqrt{2}(I^+ S^+ - I^- S^-) \qquad (15)$$

In this basis, the diagonal relaxation parameters for states $|Q_1\rangle$, $|Q_2\rangle$ have a simple physical meaning of $T_{1\rho}{}^{(1)}$, $T_{1\rho}{}^{(2)}$ longitudinal relaxation times along the respective effective locking fields, and for states $|Q_3\rangle$, $|Q_4\rangle$ the DQ relaxation time is $T_2{}^{\text{DQ}}$. The equations of motion for the expectation values of the operators in eq 15 in the vicinity of $n = 2$ DQ resonance condition will therefore look like

$$\frac{\mathrm{d}}{\mathrm{d}t}\begin{pmatrix}\langle Q_1(t)\rangle\\ \langle Q_2(t)\rangle\\ \langle Q_3(t)\rangle\\ \langle Q_4(t)\rangle\end{pmatrix} = \begin{pmatrix}-1/T_{1\rho}{}^{(1)} & & & -\sqrt{2}\omega_D^{\text{eff}}\\ & -1/T_{1\rho}{}^{(2)} & & -\sqrt{2}\omega_D^{\text{eff}}\\ & & -1/T_2{}^{\text{DQ}} & \Delta_1 + \Delta_2\\ \sqrt{2}\omega_D^{\text{eff}} & \sqrt{2}\omega_D^{\text{eff}} & -\Delta_1 - \Delta_2 & -1/T_2{}^{\text{DQ}}\end{pmatrix}\begin{pmatrix}\langle Q_1(t)\rangle\\ \langle Q_2(t)\rangle\\ \langle Q_3(t)\rangle\\ \langle Q_4(t)\rangle\end{pmatrix} \qquad (16)$$

and have to be solved with the initial condition corresponding to the initial polarization on CO: $\langle Q_1(0)\rangle = 1$, $\langle Q_2(0)\rangle = 0$, $\langle Q_3(0)\rangle = 0$, $\langle Q_4(0)\rangle = 0$. Among the four unknowns in eq 16, two longitudinal $T_{1\rho}$ relaxation times can be calibrated in a separate experiment. Far from the resonance condition, the decay of the longitudinal polarizations I_z, S_z is entirely determined by the longitudinal relaxation times. One can therefore measure the longitudinal magnetization decay from the separate $T_{1\rho}$ experiment, leaving only two unknowns in eq 16: $T_2{}^{\text{DQ}}$ and the effective dipolar coupling ω_D^{eff}. The R^{2}TRW experiment is conducted as a function of the rf intensity, $\omega_1/2\pi$, and the best fit to the experimental data can be evaluated by calculating the two-dimensional root-mean-square deviation (RMSD) according to

$$\text{RMSD}(\omega_D^{\text{eff}}, T_2^{\text{DQ}}) = \frac{1}{n}\sum_{i=1}^{n}(s_{\text{exp}}^{(i)} - s_{\text{sim}}^{(i)})^2 \qquad (17)$$

where $s_{\text{exp}}^{(i)}$ is the experimental intensity, and $s_{\text{sim}}^{(i)}$ is the theoretically predicted intensity. The total dispersion was calculated as a sum of the random and systematic dispersions.

Systematic Uncertainties in the Measured Distances. In the following section, we discuss possible systematic uncertainties of the measured distances and their sources. Specifically, we have inspected the errors that can be potentially generated by (i) the use of the approximate two-spin model, (ii) the uncertainty in $T_{1\rho}$ values, (iii) the uncertainty in the knowledge of carbonyl CSA orientation, and (iv) rf inhomogeneity and inhomogeneous line broadening. For the model peptides used in the experiments in this work, we have found that the distances can be overestimated by ~0.5−0.6 Å if the main sources of the systematic error − the uncertainty of $T_{1\rho}$ relaxation times, and the use of a simplified two-spin model − are completely neglected.

Even though by the appropriate choice of the experimental parameters we can suppress all unwanted recoupling of strong one-bond C′−Cα and two-bond C′−Cβ interactions, the multispin effects may have a profound influence on the spin-dynamics. For example, it may occur that a given carbonyl carbon has a few side chain carbons that are in close proximity and have similar chemical shifts. In this case, the recoupling is nonselective, and the use of the simplified two-spin model will be associated with certain systematic errors. To estimate these errors, and to determine how dipolar truncation is affected by the multiple quantum relaxation, we performed a set of three-spin simulations using the effective Hamiltonian in eq 8 as described in the Supporting Information. We considered a system of three spins, where spin-1 (carbonyl) is "strongly" coupled to a side chain spin-2 ($R_{12} \approx 2.9$ Å) and "weakly" coupled to another side chain spin-3. The spin-1 is initially polarized, while spin-2 and spin-3 are not. In the simulations, we calculated the signal of spin-3 as a function of the rf intensity (resonance curve) using the three-spin model, and explored its agreement with a two-spin approximation using the fitting function in eq 17. In principle, the signal of spin-3 in a three-spin simulation will depend on a number of parameters: the distances R_{12} and R_{13} between spins 1 and 2, and 1 and 3, the DQ and ZQ relaxation parameters, the chemical shift of spin 2, and the relative orientation of internuclear vectors $\mathbf{R_{12}}$ and $\mathbf{R_{13}}$. Rigorous evaluation would therefore require that the simulation be performed in a multidimensional parameter space. In this study, we restricted ourselves to the "worst case scenario", in which the influence of the multispin effects is maximized. We therefore considered the situation when (i) spins 2 and 3 have identical chemical shifts, (ii) the distance between spins 1 and 2 corresponds to the shortest three-bond distance, 2.9 Å, and the truncation effects would therefore be maximized, and (iii) the internuclear vector $\mathbf{R_{12}}$ is perpendicular to $\mathbf{R_{13}}$. In addition, we assumed that the DQ relaxation of the DQ coherences between spins 1 and 2, and spins 1 and 3, as well as the ZQ relaxation of the ZQ coherences between spins 2 and 3 are all equal. The longitudinal relaxation was neglected in the simulations.

To explore the interplay between dipolar truncation and MQ relaxation, we performed a series of three-spin simulations, where the long-range distance between spins 1 and 3 was set to $R_{13} = 4.6$ Å, and the relaxation time, $T_2{}^{\text{DQ}}$, was a variable. Figure 3 shows the dependence of the polarization transfer in the three-spin system on the DQ relaxation parameter. As expected, in the case of infinite relaxation, the weak dipolar interaction between spins 1 and 3 is truncated by the strong interaction between spins 1 and 2, resulting in significant reduction of the signal of spin-3. However, as the relaxation time becomes shorter, the truncation effect is reduced, and the polarization transfer between spins 1 and 3 becomes more efficient. Not less important is the fact that the difference between the signals of spin-3 in two- and three-spin simulations is diminished. For the practically important cases of $T_2{}^{\text{DQ}} \approx 2$, 4, 10 ms, the shape of the signal of spin-3 can be analyzed

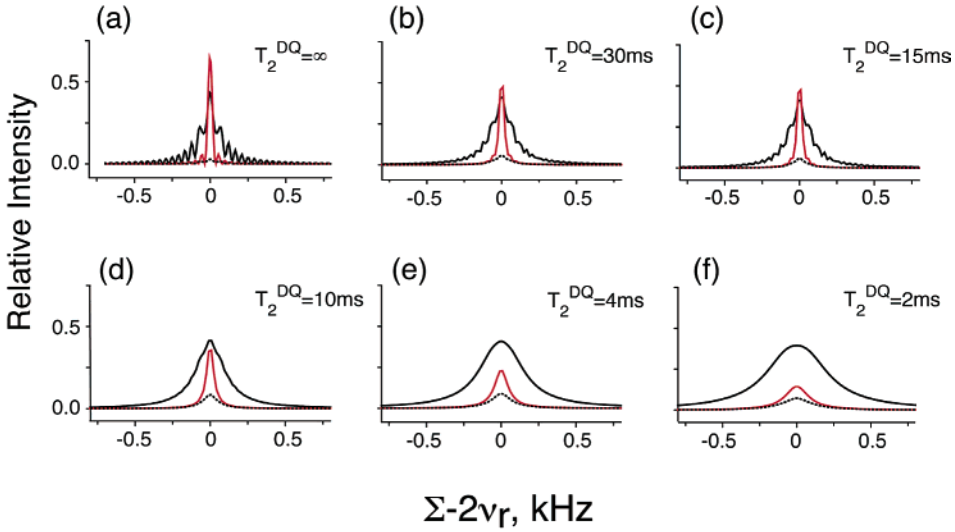

Figure 3. The dipolar truncation effect in the presence of MQ relaxation. The three-spin system was considered with $R_{12} = 2.9$ Å and $R_{13} = 4.6$ Å. The resonance shapes are plotted as a function of the deviation from the exact $n = 2$ DQ resonance condition and $\Sigma = \omega_1^{eff}/2\pi + \omega_2^{eff}/2\pi$. The upper black solid curve is always the signal of spin-2, whereas the lower black dashed line is the signal of spin-3. For comparison, the red curve represents the result of a two-spin simulation corresponding to $R_{13} = 4.6$ Å. In (a), the strong D_{12} coupling truncates the weak D_{13} interaction, leading to a significant decrease of intensity of the signal of spin-3. In (b)−(f), as relaxation becomes shorter, the signal of spin-3 grows, and the difference between the signal of spin-3 in two- and three-spin simulations is diminished. In the simulation, we assumed that the broadening of all DQ and ZQ transitions is the same; hence they can be described by a single relaxation parameter, T_2^{DQ}. The longitudinal relaxation $T_{1\rho}$ was neglected in the simulations.

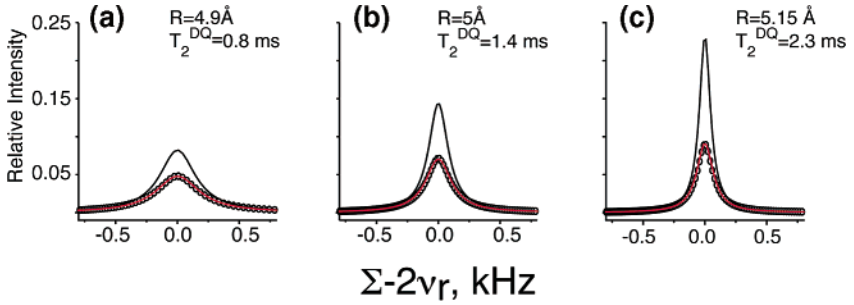

Figure 4. A comparison of the signal of spin-3 in two- and three-spin simulations for practically important values of T_2^{DQ}. The black curve represents the result of the two-spin system simulation, while the circles are the result of the three-spin simulation. The geometry of the three-spin system was as in Figure 3 with $R_{12} = 2.9$ Å and $R_{13} = 4.6$ Å. The DQ relaxation times in the three-spin simulation were $T_2^{DQ} = 1$ ms in (a), $T_2^{DQ} = 2$ ms in (b), and $T_2^{DQ} = 4$ ms in (c). The red curve represents the best fit to the signal of spin-3 in the three-spin simulation, obtained using the two-spin model. The best-fit distances and the T_2^{DQ} relaxation times extracted from the best (two-spin) fit are indicated in the figure. The extracted distances appear to be longer because of the neglect of the multiple spin effects. The DQ relaxation parameters also appear to be somewhat shorter than the input parameters.

using the two-spin simulation, and the best-fit distance is relatively close to the true distance. This is illustrated in Figure 4, where the signal of spin-3 is shown for the input $T_2^{DQ} = 1$, 2, and 4 ms, respectively, with the best fit obtained using the two-spin simulation. The systematic error is never greater than 15%.

Further simulations (results not shown) demonstrate that once relaxation is short, $T_2^{ZQ} = T_2^{DQ} \approx 2$ ms, the value of the strong dipolar coupling has a small effect on the systematic error and is always on the order of 0.4 Å. Note that the neglect of these multispin effects always results in an underestimation of the dipolar couplings.

The truncation of the weak D_{13} dipolar coupling by the strong D_{12} interaction will also be affected by the chemical shift of spin-3. So far we have assumed that spins 2 and 3 have equal chemical shifts and the resonance conditions (eq 6b) for $i = 1$, $j = 2,3$ are therefore satisfied simultaneously. If the chemical shifts of spins-2 and 3 are very different, we may expect that $1 \rightarrow 2$ and $2 \rightarrow 3$ polarization transfer processes will become independent. Indeed, when the chemical shift difference between spins-2 and 3 becomes comparable or larger than the resonance width (largely dominated by the DQ relaxation), the $1 \rightarrow 2$ and $2 \rightarrow 3$ polarization transfer processes become nearly independent, and the neglect of multispin effects results in minimal errors.

Uncertainties Due to Undefined $T_{1\rho}$ Relaxation. So far, the effects of the longitudinal relaxation were neglected. In a real experimental situation, the application of the weak rf field may result in some unwanted recoupling processes, for example, $n = 1$ DQ conditions between aliphatic spins Cα and Cγ,δ. These processes may depend on the choice of the carrier position, as well as on the rf amplitude. In addition, the magnetization of the carbonyl carbons will be influenced by the part of the CSA Hamiltonian in eq 3 that does not commute with the effective field. These effects may result in additional signal decay and were taken into account phenomenologically by introducing effective $T_{1\rho}$ relaxation times. In practice, $T_{1\rho}$ calibration experiments may be performed at rf intensities that do not lead to any resonance conditions (eq 6b). For example, the $T_{1\rho}$ calibration at high and low rf intensities, that is, above and below DQ resonance conditions, provides lower and upper bounds on the $T_{1\rho}$ relaxation parameter and can be used to

estimate the systematic error due the undefined relaxation. It is instructive, however, to estimate a systematic error introduced if the $T_{1\rho}$ effects are completely neglected.

To accomplish this, we generated a number of curves for different distances using $T_2^{DQ} = 2$ ms, and rather short longitudinal relaxation times of $T_{1\rho}^{(1)} = T_{1\rho}^{(2)} = 40$ ms, the shortest among those observed experimentally. In the fit simulation, the longitudinal relaxation was neglected. Neglecting relaxation results in an underestimate of the dipolar interaction. We found that this underestimate is rather universal in the range of distances 3−4.5 Å and is ∼0.6 Å for the relaxation parameters chosen here. The uncertainty in the dipolar coupling resulting from the uncertainty of relaxation is further discussed in the Experimental Section.

Uncertainties Due to Undefined CSA Orientation. For the spinning frequencies required to conduct the $n = 2$ DQ R^2-TRW experiments and typically observed MQ relaxation times, the CSA orientation effects have no significant influence on the observed resonance line shapes. Simulations performed showed no appreciable change of the resonance shape as a function of CSA orientation. In addition, the scaling of the dipolar interaction (eq 10) depends on the ratio of the CSA strength and the spinning frequency. This ratio is independent of the B_0 field, and we can therefore expect that the CSA orientation effects will be negligible at all B_0 fields.

Uncertainties Due to rf Inhomogeneity and Sample Heterogeneity. The R^{2}TRW experiment is fairly insensitive to the rf inhomogeneity (we assumed 10% rf inhomogeneity and observed no significant change from the "homogeneous" case). The effect of the B_0 inhomogeneity is also rather small. To estimate this effect, the following simulation was performed. We first assumed that the isotropic chemical shift of spin-2 in a two-spin simulation is distributed according to a Lorentzian function with a typical width of 0.1 kHz and calculated the resonance shape assuming a distance $R_{12} = 4$ Å and a relaxation time $T_2^{DQ} = 2$ ms. This resonance shape was fit using two-spin simulation while neglecting the B_0 inhomogeneity effects. The best-fit distance appeared 0.1 Å longer, much smaller than other sources of systematic error discussed above.

To summarize the possible systematic errors discussed here, we note that the most significant ones are the uncertainty in longitudinal relaxation times and the use of a simplified two-spin model. They may result in the underestimation of internuclear distances. However, if the side chain spectral lines are resolved, and there is, therefore, selectivity of the polarization transfer, and also there is some information about longitudinal relaxation times, the distances can be determined relatively accurately, with a precision of 15−20%.

Experimental Results and Discussion

Distance Measurements in *N*-Acetyl-[U-^{13}C,^{15}N]Val-Leu. Here, we apply the 3D R^{2}TRW experiment to carbonyl−side chain distance measurements. In the first pulse sequence investigated here, the experiment is combined with ^{13}C−^{13}C correlation spectroscopy for site-specific determination of distance constraints and applied in *N*-acetyl-[U-^{13}C,^{15}N]Val-Leu. The three-dimensional structure of a peptide has been determined using X-ray crystallography and is shown in Figure 5.[61]

(61) Carroll, P. J.; Stewart, P. L.; Opella, S. J. *Acta Crystallogr.* **1990**, *C46*, 243−246.

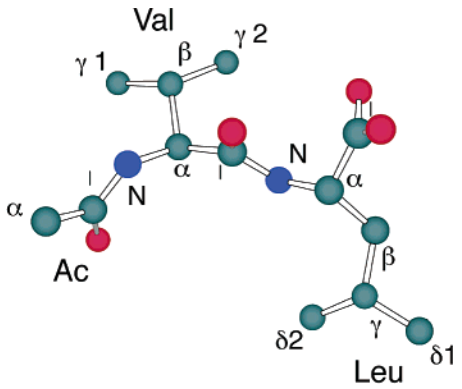

Figure 5. X-ray crystal structure of *N*-acetyl-L-Val-L-Leu.[61]

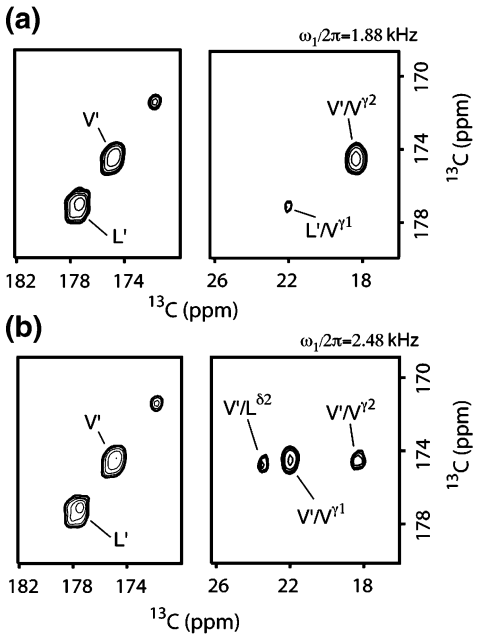

Figure 6. Representative two-dimensional slices from the ^{13}C−^{13}C R^2-TRW experiment in *N*-acetyl[U-^{13}C,^{15}N]L-Val-L-Leu obtained on a 360 MHz spectrometer. The pulse sequence of Figure 1a was used with the carrier frequency set between carbonyl and side chain resonances, such that $|\Delta\omega_\beta| + |\Delta\omega_\gamma| > \omega_R$ for all β- and γ-resonances to avoid DQ recoupling between them. The mixing time of 25 ms was used in the experiment. The spinning frequency was 7.4 kHz. 192 complex points were taken in the t_1 dimension with the increment of 50 μs and 16 acquisitions per point. 30 points were taken in the $\omega_1/2\pi$ dimension in the range 0.8−4.2 kHz. Different cross-peaks appear at different rf intensities, demonstrating the selectivity of the polarization transfer. In (a), a strong cross-peak corresponding to the short-range V′−Vγ2 dipolar coupling ($R = 2.96$ Å according to a crystal structure) appears in the spectrum, along with long-range coupling between the L′ and Vγ1 ($R = 6.45$ Å). In (b), two more cross-peaks are observed between V′ and Vγ1 ($R = 3.89$ Å) and V′ and Lδ2 ($R = 4.29$ Å), while the V′−Vγ2 cross-peak intensity is significantly reduced.

The spectral assignments for this peptide have also been reported previously.[27]

The R^{2}TRW experiments were performed at 360 MHz (proton frequency) and at a spinning rate of 7.4 kHz. The ^{13}C spectrum for this peptide is shown in Figure 2, and in Figure 6 we show representative two-dimensional slices from the R^{2}TRW experiment corresponding to rf amplitudes of 1.88 and 2.48 kHz. For clarity, only carbonyl diagonal peaks and carbonyl−side chain cross-peaks are shown. The cross-peaks in the aliphatic region are labeled with the carbonyl and side chain carbon frequencies.

The spectra were acquired using pulse sequence in Figure 1a. The aliphatic part of the spectra clearly demonstrates the

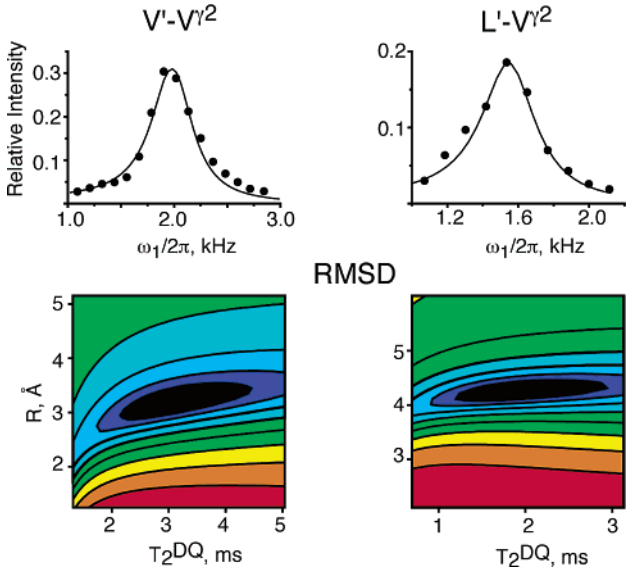

Figure 7. Representative plots of the cross-peak intensities as a function of the rf power for V′−Vγ2 and L′−Vγ2 resonances, and corresponding RMSD contour plots. The volume intensities of the cross-peak are given relative to the corresponding carbonyl peaks. The parameters in these simulations were as follows. For V′−Vγ2: $T_{1\rho}^{(1)} = 90$ ms, $T_{1\rho}^{(2)} = 80$ ms, $T_2^{DQ} = 3.2$ ms, $R = 3.2$ Å. For L′−Vγ2: $T_{1\rho}^{(1)} = 616$ ms, $T_{1\rho}^{(2)} = 188$ ms, $T_2^{DQ} = 2.4$ ms, $R = 4.3$ Å. The first contour corresponds to a 95% confidence level. The plots were fit using a two-spin model as explained in the text.

Table 1. Longitudinal Relaxation Times for Different Lines in N-Ac-VL Determined at Different rf Intensities

	$T_{1\rho}$, ms	
line	($\omega_1/2\pi = 0.9$ kHz)	($\omega_1/2\pi = 4$ kHz)
L′	616	40
V′	395	48
Lγ	97	24
Lδ1	71	54
Lδ2	80	40
Vγ1	237	60
Vγ2	188	63

selectivity of the polarization transfer. For $\omega_1/2\pi = 1.88$ kHz, only the cross-peak corresponding to polarization transfer between V′ and Vγ2 carbons appears, whereas at $\omega_1/2\pi = 2.48$ kHz, the intensity of this cross-peak is diminished, and the cross-peaks corresponding to V′−Vγ1 and V′−Lδ2 dipolar contacts appear in the spectra. The cross-peak intensities are characteristic of the dipolar coupled carbonyl−side chain spin pairs and can be used to estimate dipolar interactions between them. This estimate requires knowledge of the longitudinal relaxation time, $T_{1\rho}$. As explained in the theoretical section, the calibration of the $T_{1\rho}$ requires experimental conditions at which the longitudinal magnetization decay will be determined by the relaxation alone. In N-Ac-VL, all recoupling conditions for CO−Cβ/γ/δ spin pairs require application of the rf field between ∼1.5 kHz (for L′−Vγ2 spin pair) and ∼3.6 kHz (V′−Lβ spin pair). The $T_{1\rho}$ calibration experiments were therefore conducted at $\omega_1/2\pi = 0.9$ and 4 kHz, below and above all recoupling conditions. The values of the measured relaxation times are given in Table 1.

These values were used as lower and upper bounds on longitudinal relaxation times and are the main source of the systematic error. The dependence of the cross-peak intensity on the rf field is shown in Figure 7 for V′−Vγ2 and L′−Vγ2

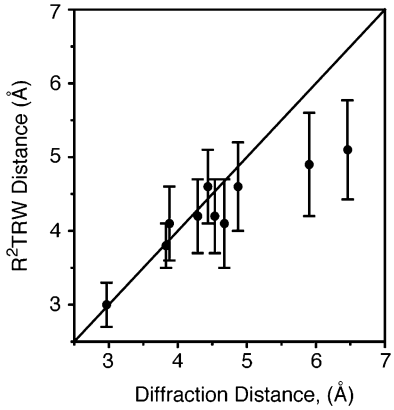

Figure 8. Comparison of $^{13}C-^{13}C$ distances measured by using X-ray diffraction and R²TRW experiments. The NMR result accounts for major sources of systematic error: inaccurate knowledge of longitudinal relaxation effects and multispin effects.

Table 2. Internuclear Distances Measured in *N*-Ac[U-^{13}C,^{15}N]L-Val-L-Leu

atoms		$^{13}C-^{13}C$ distance (Å)	
		R²TRW	X-ray
V′	Vγ2	2.7−3.3	2.969
	Vγ1	3.6−4.6	3.879
	Lδ1	3.7−4.7	4.290
	Lδ2	4.2−5.6	5.902
	Lγ	4.1−5.1	4.436
L′	Vγ2	3.7−4.7	4.535
	Vγ1	4.4−5.8	6.46
	Lδ1	3.8−4.8	4.675
	Lδ2	4.0−5.2	4.872
	Lγ	3.5−4.2	3.829

spin pairs together with the best-fit simulations and RMSD plots. The peak intensities are referenced with respect to the intensity of the carbonyls where the polarization transfer initiated.

As can be seen from the RMSD plots, the distances can be localized from these plots with relatively high precision. The carbonyl−side chain distance measurements are summarized in Figure 8 and Table 2. A total of 10 distances were measured in this dipeptide using pulse sequence in Figure 1a. As pointed out above, the relatively large error bars are due to uncertainty in the longitudinal relaxation time, $T_{1\rho}$.

In addition, our measurements tend to yield distances shorter than X-ray for weak couplings (V′−Lδ2, L′−Vγ1). This may be due to residual intermolecular couplings that may be stronger than intramolecular interactions. We notice that similar effects were observed in 3D TEDOR measurements performed on peptides with similar dilution.[33]

Distance Measurements in [U-^{13}C,^{15}N]N-*f*-MLF-OH. The analysis of the experimental data obtained in the N-Ac-VL sample presented above relied on the fact that the carbonyl region of the spectrum is completely resolved. An accurate knowledge of the carbonyl intensities is desirable because they serve as a reference for the initial conditions. In most systems of interest, the resolution of carbonyl spectral region is very limited. Further improvement of spectral resolution can be achieved by including the ^{15}N chemical shift dimension, using the pulse sequence illustrated in Figure 1b. This pulse sequence starts with cross-polarization that creates transverse magnetization on the ^{15}N channel. The ^{15}N magnetization is frequency labeled in the t_1 dimension and then selectively transferred to

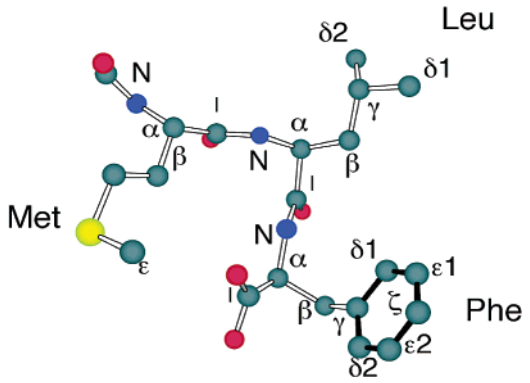

Figure 9. ssNMR structure of N-*f*-MLF-OH.[24]

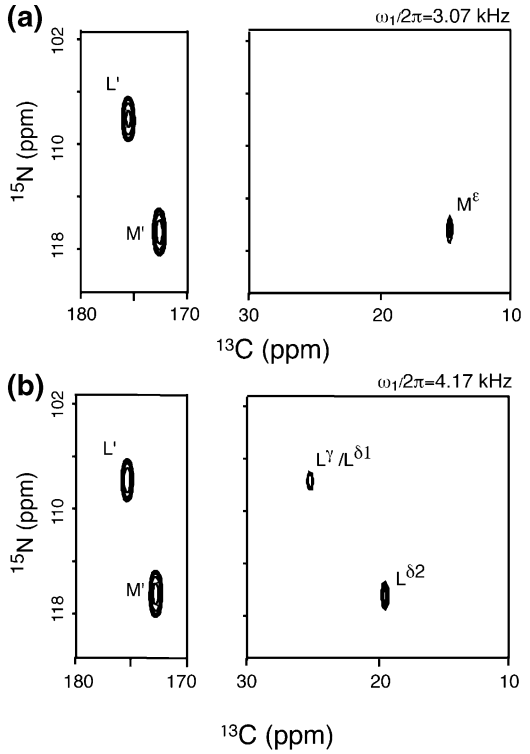

Figure 10. Representative two-dimensional slices from the $^{13}C-^{15}N$ R^2-TRW experiment in *N*-formyl[U-^{13}C,^{15}N]L-Met-L-Leu-L-Phe obtained on a 500 MHz spectrometer. The spinning frequency was 10.5 kHz in this experiment. The pulse sequence of Figure 1b was used with the carrier frequency set between carbonyl and side chain resonances. The mixing time of 40 ms was used in the experiment. 16 complex points were taken in the t_1 dimension with the increment of 476.2 μs and 128 acquisitions. 70 points were taken in the $\omega_1/2\pi$ dimension in the range 2.1−5.4 kHz (15−20 points per resonance shape). Note that the number of points in the $\omega_1/2\pi$ dimension could have been reduced by a factor of 2−3 without significant loss of accuracy. Different cross-peaks appear at different rf intensities, demonstrating the selectivity of the polarization transfer. In (a), a long-range cross-peak M′−Mϵ (R = 5.52 Å according to a ssNMR structure[24]) appears in the spectrum. In (b), intermediate range couplings result in cross-peaks due to L′−Lγ/Lδ1 (R = 3.8 or 4.2 Å, respectively) and an interresidue M′−Lδ2 (R = 4.07 Å) cross-peak.

the carbonyl carbons of the preceding residues. Therefore, the NCO spectrum represents a reference for the aliphatic peak intensities. The polarization is then transferred from carbonyls to side chain carbons during the constant time R^{2}TR mixing step. The experiment has been tested in the tripeptide N-*f*-MLF-OH at a ^1H frequency of 500 MHz and at a spinning rate of 10.5 kHz. The assignments for this tripeptide have been published previously,[55] as has its molecular structure[24] which

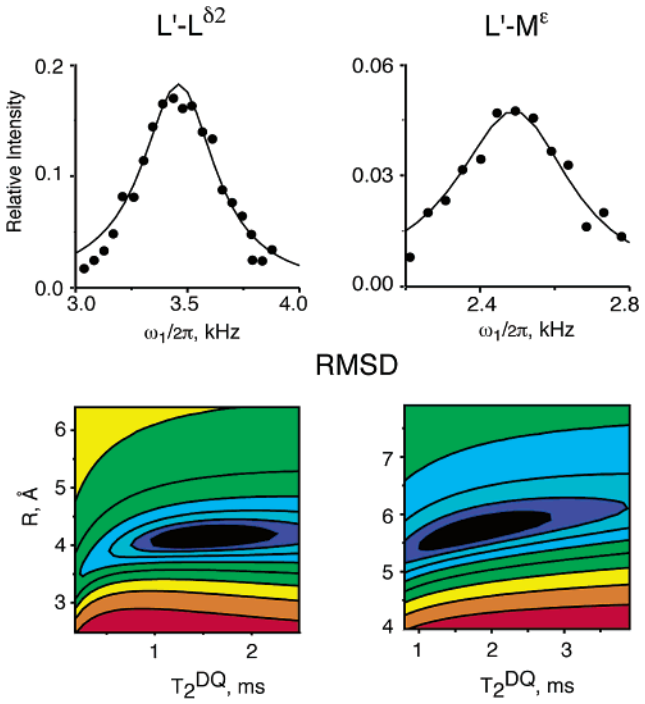

Figure 11. Representative plots of cross-peak intensities as a function of rf power for L′−Lδ2 and L′−Mϵ resonances, and corresponding RMSD contour plots. The first contour corresponds to a 95% confidence level. The plots were fit using a two-spin model as explained in the text. The best fits shown here were calculated using long $T_{1\rho}$ relaxation times of 412 and 254 ms for L′ and Lδ2 resonances (best-fit distance, R = 4.4 Å), respectively, and 412 and 315 ms for L′ and Mϵ (best-fit distance, R = 5.7 Å).

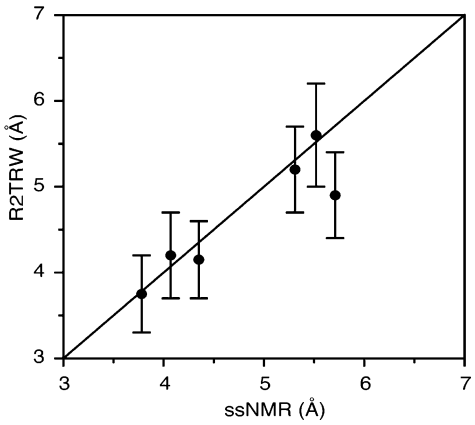

Figure 12. Comparison of $^{13}C-^{13}C$ distances measured by using R^{2}TRW experiments presented here, and by other ssNMR methods.[24] R^{2}TRW results account for major sources for systematic error: inaccurate knowledge of relaxation effects and multispin effects.

was obtained by using ssNMR torsion angle methods[23] and $^{13}C-^{15}N$ distance measurement techniques.[27] This structure is shown in Figure 9.

The spectra in Figure 10 represent 2D slices of a 3D experiment for $\omega_1/2\pi$ = 3.07 and 4.17 kHz, respectively. The NCO cross-peaks are labeled according to the carbonyl assignment, and the cross-peaks in the aliphatic region are labeled according to the chemical shifts of the interacting spin pair. Similar to a previous example, the appearance of the cross-peaks in the aliphatic region is indicative of the dipolar interactions between corresponding atoms. The aliphatic cross-peaks corresponding to M′−Mϵ, M′−Lδ2, and L′−Lγ/Lδ1 dipolar interactions build up at different rf intensities, a

Table 3. Longitudinal Relaxation Times for Different Lines in [U-^{13}C,^{15}N]N-*f*-MLF-OH Determined at Different rf Intensities

	$T_{1\rho}$, ms	
line	($\omega_1/2\pi = 1.13$ kHz)	($\omega_1/2\pi = 5.16$ kHz)
L′	412	74
M′	600	50
Mγ	212	72
Lδ2	254	78
Mϵ	315	40

Table 4. Internuclear Distances Measured in *N*-Formyl-L-Met-L-Leu-L-Phe-OH

		^{13}C–^{13}C distance (Å)	
atoms		R^{2}TRW	ssNMR
M′	Mγ	3.3−4.2	3.78
	Mϵ	4.7−5.7	5.31
	Lδ2	3.7−4.7	4.07
L′	Mγ	4.4−5.4	5.71
	Mϵ	5.0−6.2	5.52
	Lδ2	3.7−4.6	4.35

manifestation of the chemical shift-based polarization transfer selectivity. The examples of the observed resonances are shown in Figure 11 for L′−Lδ2 and L′−Mϵ spin pairs together with the corresponding RMSD plots.

Similar to the N-Ac-VL case, the longitudinal relaxation times were measured at low and high rf intensities, where no recoupling was observed. These values are shown in Table 3 and were used in the simulations as lower and upper estimates on relaxation.

Again, the RMSD plots in Figure 11 demonstrate that the distances can be constrained with relatively high precision for a given set of $T_{1\rho}$ relaxation times. A total of six distances were determined in this experiment. The results of the R^{2}TRW measurements are compared with the previously published ssNMR 3D structure[24] in Figure 12 and Table 4.

Conclusion

We have presented 3D R^{2}TRW experiments for the simultaneous site-specific measurement of multiple carbonyl−side chain ^{13}C−^{13}C distances in uniformly ^{13}C,^{15}N-labeled solids. The attractive feature of these experiments is that they allow independent experimental extraction of the dipolar coupling and the multiple-quantum relaxation parameters and are therefore free of ambiguities associated with the presence of MQ relaxation. The experiments have been demonstrated in N-Ac-VL and N-*f*-MLF-OH model peptides, where 10 and 6 intra- and interresidue distances in a range between 2.9 and 6 Å were measured, respectively. Two-spin and three-spin models, used for data analysis, lead to similar results. The experiments were conducted at moderate spinning frequencies just above $n = 2$ R^2 conditions. We expect that at higher spinning frequencies above $n = 1$ rotational resonance, the experiment will perform better due to the fact that most of the "parasitic" recoupling conditions that lead to $T_{1\rho}$ effects are avoided.

A quantitative analysis of the cross-peak intensities requires resolution of the carbonyl spectrum. In proteins, this region of the spectrum is usually not well resolved. Approaches to enhance the resolution by combining the R^{2}TRW experiment with ^{15}N−^{13}C correlation spectroscopy were discussed. However, we would like to stress that even in a scenario when the spectra lack resolution, and longitudinal relaxation is unknown, the presence of cross-peaks in ^{13}C−^{13}C or ^{13}C−^{15}N spectra obtained using pulse sequences in Figure 1a or b, respectively, provides direct information about spatial proximities of carbonyl and side chain carbons. In cases when these cross-peaks correspond to interresidue interactions, they are directly related to a three-dimensional structure of a molecule.

We expect the R^{2}TRW experiments presented here to be applicable to structural measurements in noncrystalline biological solids, such as membrane proteins and insoluble peptide aggregates. In systems of these types, additional sources of systematic errors must be considered, in particular, molecular motion. The dynamic processes, especially for the side chains, can partially average dipolar couplings, leading to longer NMR-determined distances.[62] The type of molecular motion, its rate, etc. will likely determine the exact nature of averaging. These factors should be taken into account when interpreting the data of distance measurements.

The principles of selective recoupling and the "resonance width" approach can also be used to estimate structurally important methyl−methyl dipolar contacts, as well as ^{15}N−^{13}C dipolar interactions. These methods are currently being developed in our laboratory.

Acknowledgment. We thank Mr. Vikram Bajaj for careful reading of the manuscript and for stimulating discussions, and Dr. Claudiu Filip for useful advice. This research was supported by NIH grants GM23403 and RR00995/EB001960.

Supporting Information Available: Description of simulations used to estimate multispin effects (PDF). This material is available free of charge via the Internet at http://pubs.acs.org.

JA037138C

(62) Langlais, D. B.; Hodges, R. S.; Davis, J. H. *Phys. Rev.* **1999**, *E59*, 5945−5957.